

Supporting Information

Electronic tuning in WSe₂/Au via van der Waals interface twisting and intercalation

Qilong Wu, † Meysam Bagheri Tagani, ‡ Lijie Zhang, † Jing Wang, † Yu Xia, † Li Zhang, † Sheng-Yi Xie, † Yuan Tian, † Long-Jing Yin, † Wen Zhang, § Alexander N. Rudenko, || Andrew T.S. Wee, ††, ‡‡ Ping Kwan Johnny Wong, §* and Zhihui Qin†**

†Key Laboratory for Micro/Nano Optoelectronic Devices of Ministry of Education & Hunan Provincial Key Laboratory of Low-Dimensional Structural Physics and Devices, School of Physics and Electronics, Hunan University, Changsha 410082, People's Republic of China

‡Department of Physics, University of Guilan, P.O. Box 41335-1914, Rasht, Iran

§School of Microelectronics, Northwestern Polytechnical University, Xi'an 710072, Shaanxi & NPU Chongqing Technology Innovation Center, Chongqing 400000, People's Republic of China

||Institute for Molecules and Materials, Radboud University, Heijendaalseweg 135, 6525 AJ Nijmegen, The Netherlands

††Department of Physics, National University of Singapore, 2 Science Drive 3, Singapore 117551, Singapore

‡‡ Centre for Advanced 2D Materials (CA2DM) and Graphene Research Centre (GRC), National University of Singapore, 6 Science Drive 2, Singapore 117546, Singapore

*Email: lijiezhang@hnu.edu.cn; pingkwanj.wong@nwpu.edu.cn; zhqin@hnu.edu.cn

The supporting information includes Figures S1-S12

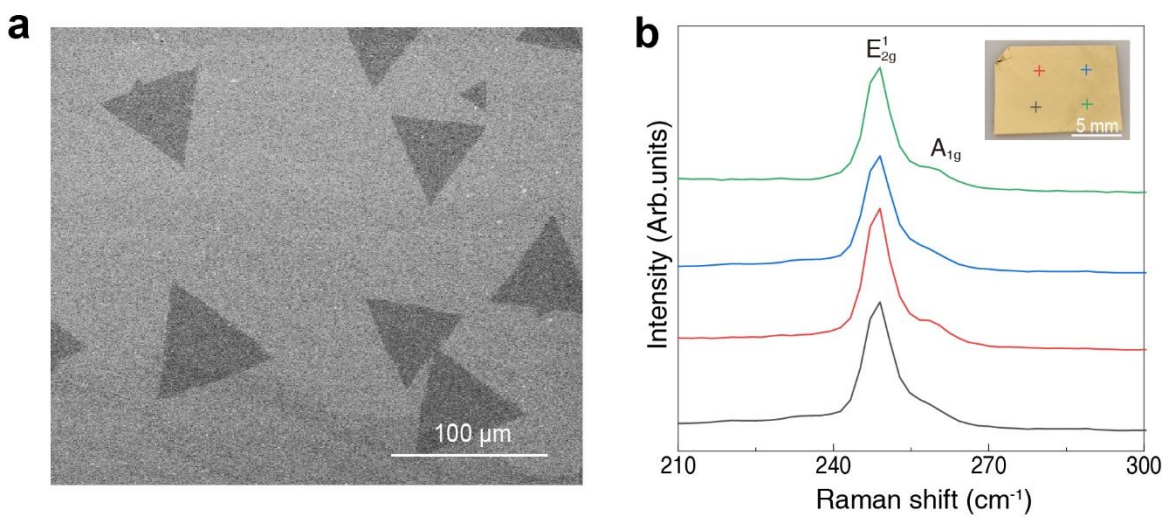


Figure S1. (a) SEM image of large WSe₂ thin film grown on Au foil by CVD. (b) The Raman spectra determine the quality homogeneity of the monolayer WSe₂ sample. The crosses in the inset correspond to the positions of the Raman spectra.

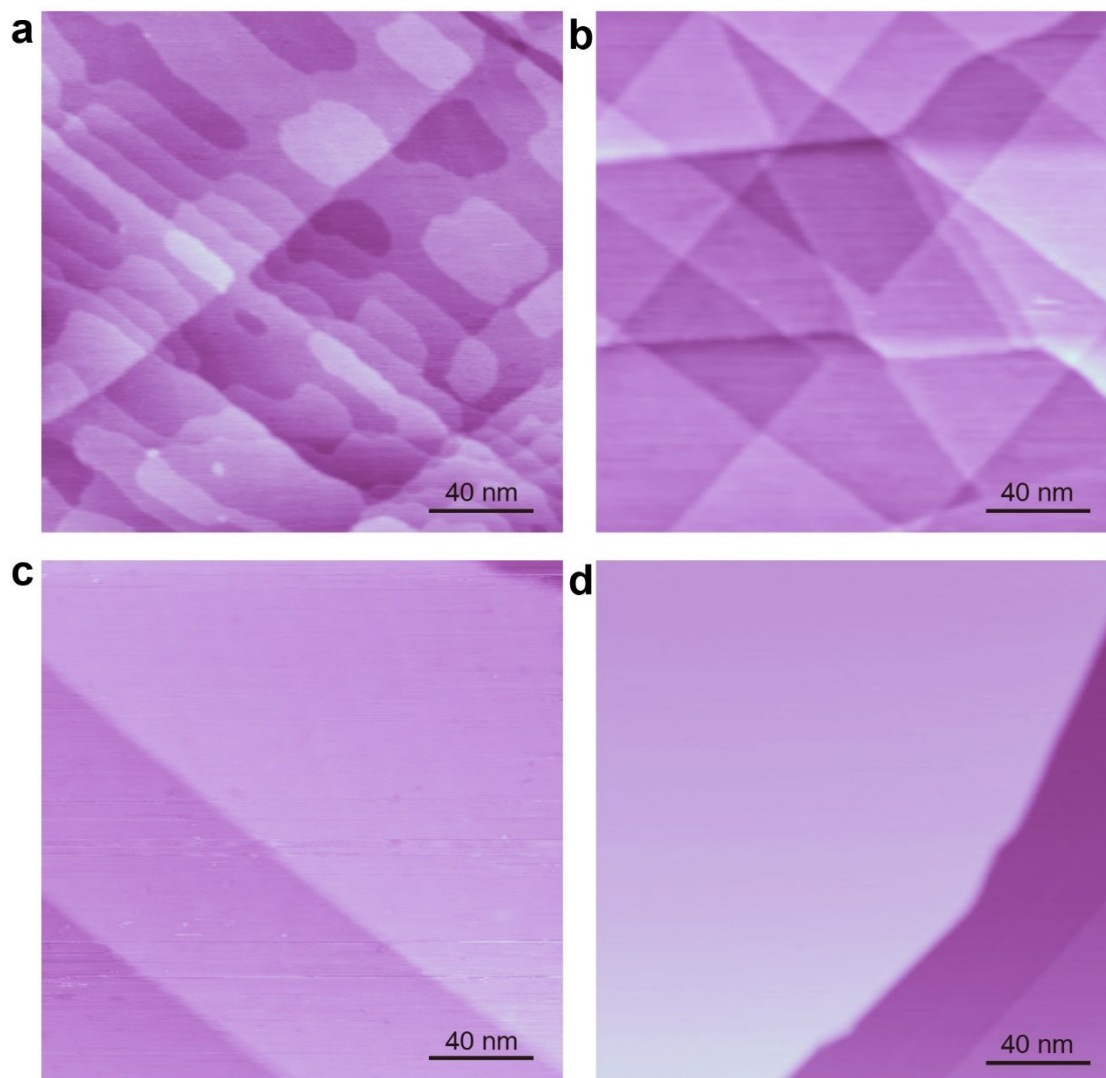


Figure S2. Large-scale STM images of WSe₂/Au(100) annealed at different temperatures in ultra-high vacuum. Images (a), (b), (c) and (d) correspond to 450 K degassing for 30 minutes, 650 K annealing for 15 minutes, 670 K annealing for 30 minutes, and 720 K annealing for 30 minutes. (a) Sample bias 1 V, tunnel current 4 pA. (b) Sample bias 1.8 V, tunnel current 2 pA. (c) Sample bias -2 V, tunnel current 5 pA. (d) Sample bias -2 V, tunnel current 1 pA.

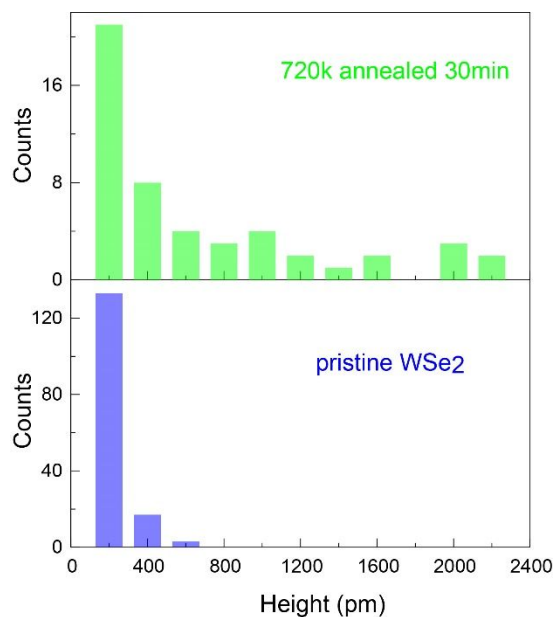


Figure S3. The statistical step height distribution images are the unannealed WSe₂ surface and the WSe₂ surface after 720k annealing for 30 min. Among them, the unannealed surface randomly counts 150 step heights. After annealing, because the surface becomes very flat, the number of steps decreases, and only 50 randomly counts.

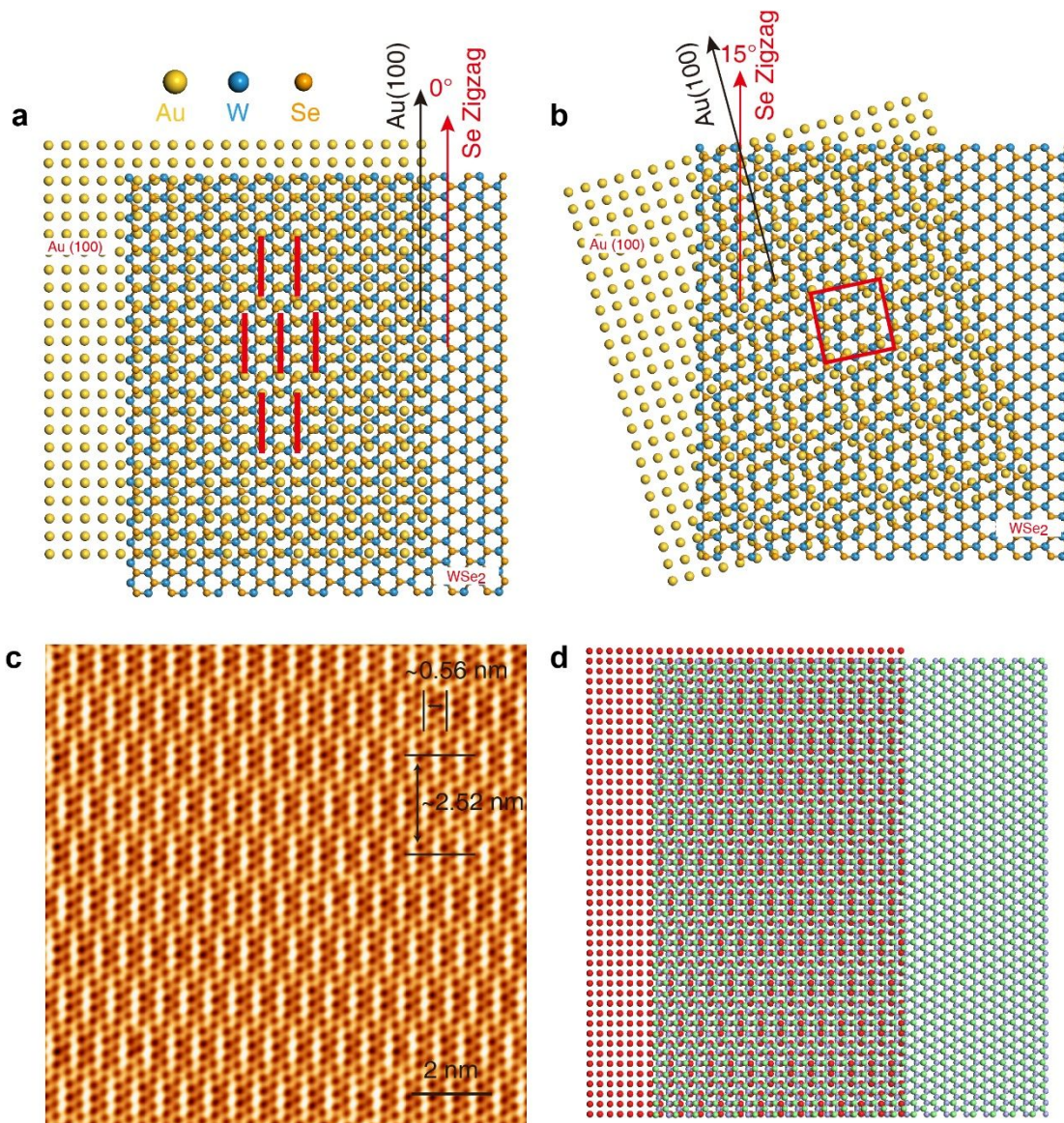


Figure S4. (a) and (b) correspond to the Au (100) lattice direction (black arrow) and the Se-zigzag direction of WSe₂ (red arrow), respectively. (c) Large-scale STM image with a rotation angle of 0°, and its period length is marked in the figure, corresponding to the simulation diagram of (d). (c) Sample bias -50 mV, tunnel current 1 nA.

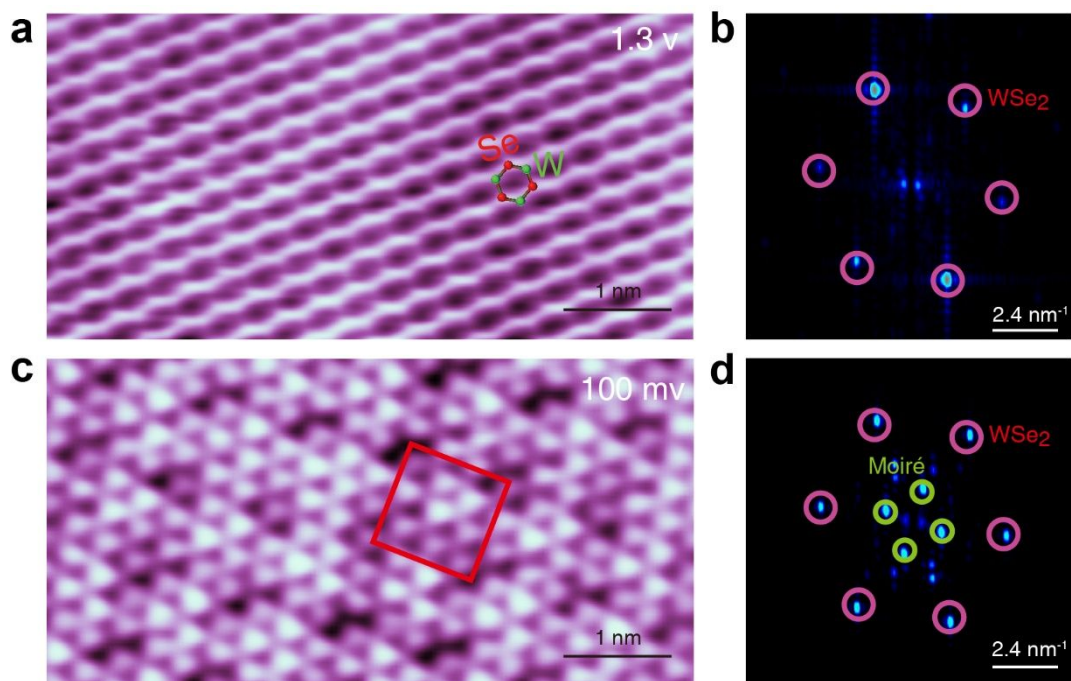


Figure S5. Bias voltage dependence of 15°-twist WSe₂/Au(100) moiré structure. (a) and (c) The STM images of 15°-twist WSe₂/Au(100) under different bias voltages, (a) Sample bias 1.3V and tunnel current 100 pA. (c) Sample bias 100 mV and tunnel current 500 pA. (b) and (d) correspond to the fast Fourier transition (FFT) of (a) and (c). It can be found that the moiré structure disappears at high bias voltage.

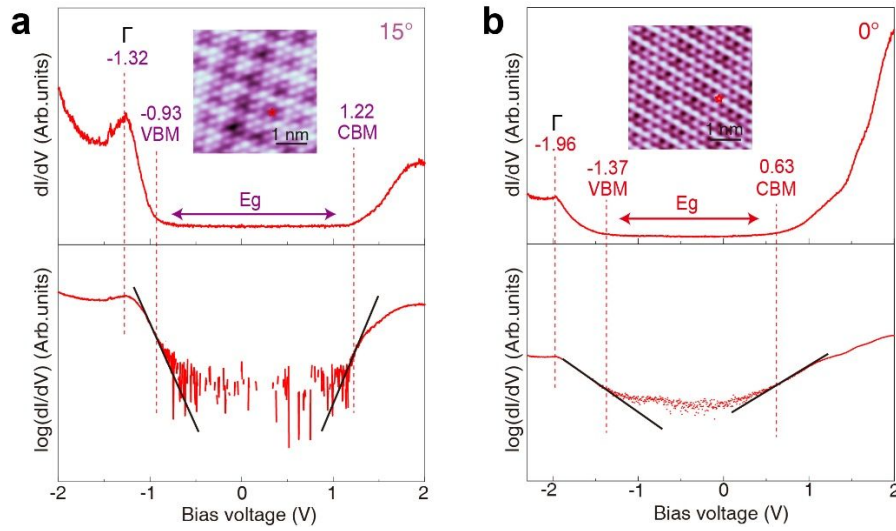


Figure S6. (a) and (b) refer to the 15°- and 0°-twist WSe₂/Au(100) dI/dV spectra, respectively, and the logarithmic dI/dV spectra are at the bottom panels. The method is similar to a previous report¹.

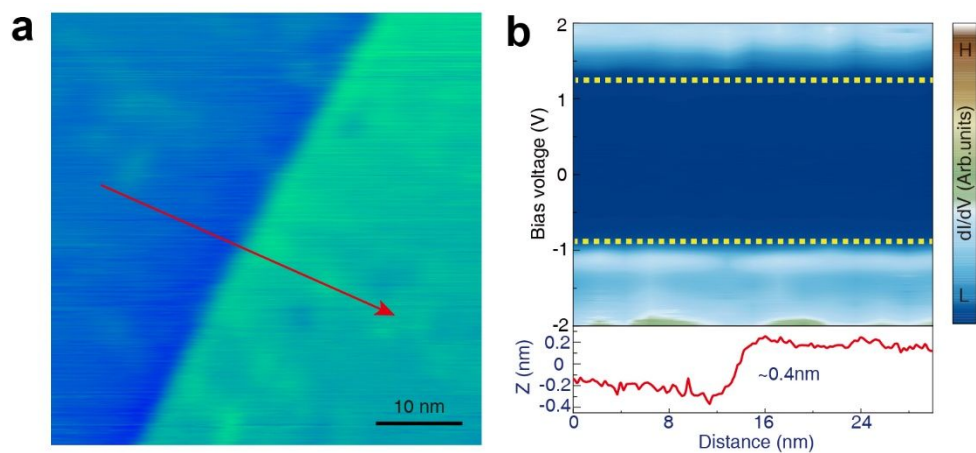


Figure S7. (a) STM image of the unannealed WSe₂ surface. The dI/dV spectrum of WSe₂ across the steps is collected along the gold step with a height of 0.4 nm, and the dI/dV is mapped to color and drawn in (b). It can be clearly seen that no significant changes have been found in the electronic properties of WSe₂ across the step. (a) Sample bias 1.8V, tunnel current 10 pA.

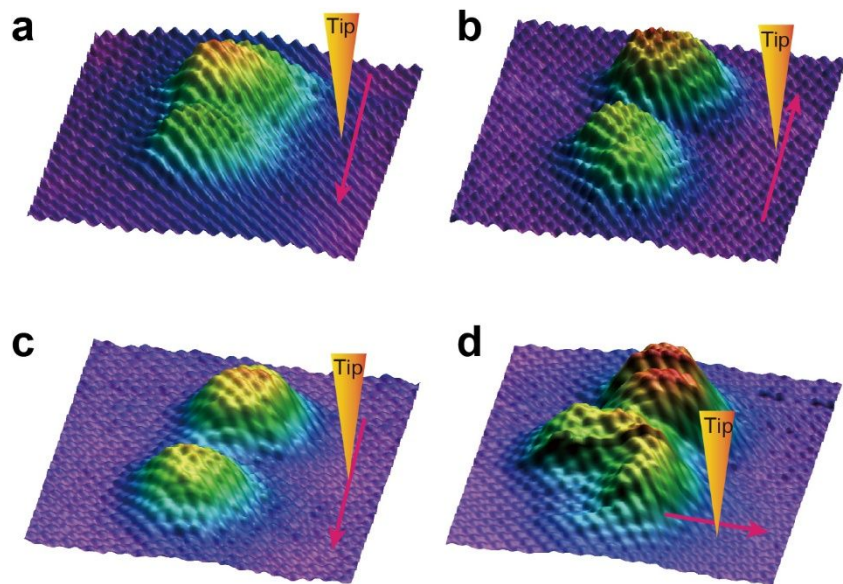


Figure S8. 3D image of WSe_2 surface after germanium intercalation. Corresponding to the text in Figure 4d. The scanning direction map of the tip is shown in the figure.

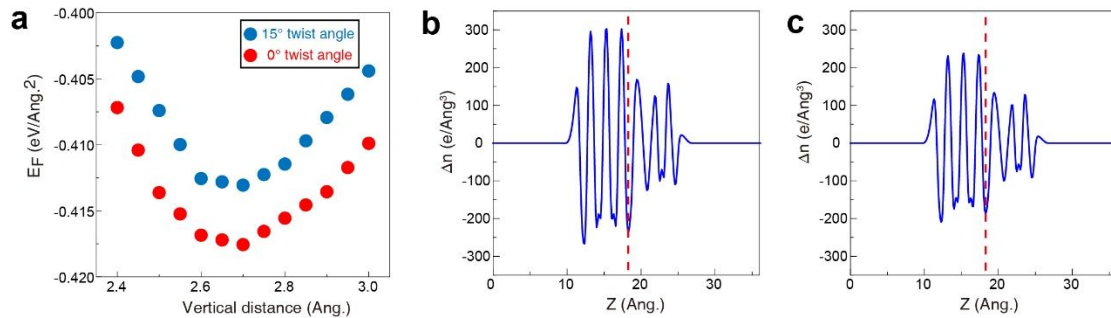


Figure S9. (a) Variation of formation energy versus vertical distance between Au slab and monolayer WSe₂ for both 0° and 15° twisted structures. (b) and (c) The averaged electron density difference for twist angle of 0° and 15°, respectively. The dashed line shows the position of topmost Au layer along z direction.

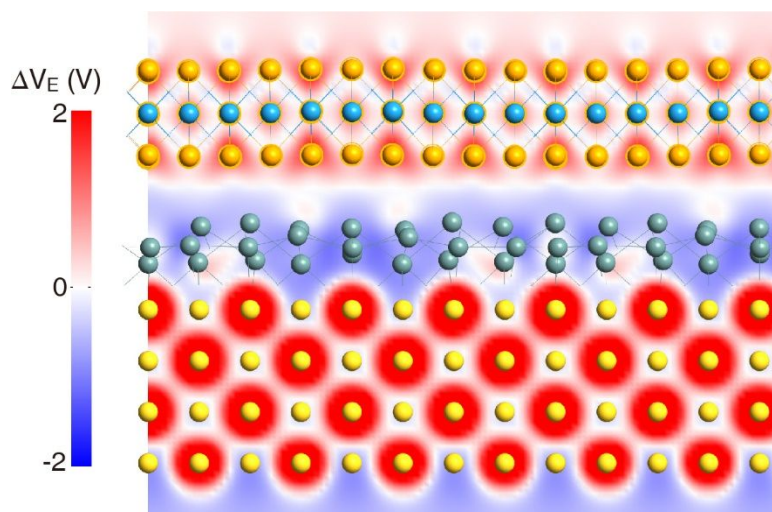


Figure S10. Electrostatic potential difference for Ge intercalated 0° twist $\text{WSe}_2/\text{Au}(100)$ heterojunction.

The WSe₂ electronic character was also seen to change due to the moiré transformation. Figure S11 for instance, highlights how the carrier concentration and even the doping type vary with annealing temperature. When the temperature increases, the initial n-type doping concentration of WSe₂ increases. Annealing inevitably creates some defects², though, as shown in Figure S12. Below 750 K, a defect concentration remains at the level of $\sim 3.3 \times 10^{11} \text{ cm}^{-2}$, but increases significantly to $1.5 \times 10^{12} \text{ cm}^{-2}$ for 800 K. Therefore, we can safely rule out the defect contribution to the observed doping change for annealing at or below 700 K. This also suggests that high temperature treatment will make WSe₂ more metallic and reduces its band gap. Consequently, the thermal treatment needs to be controlled within an appropriate temperature and time window, in order to effectively switch the WSe₂ doping from p-type to n-type.

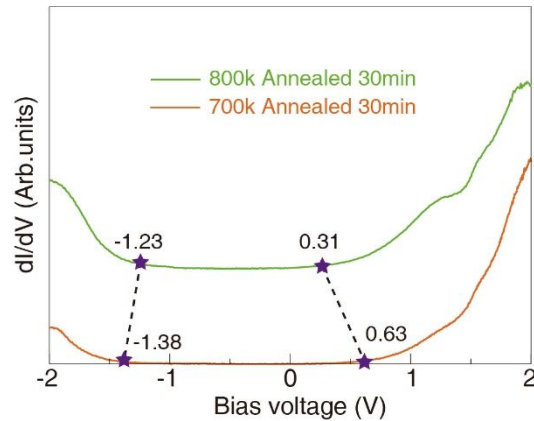


Figure S11. dI/dV spectra obtained by annealing the samples in ultrahigh vacuum at different temperatures.

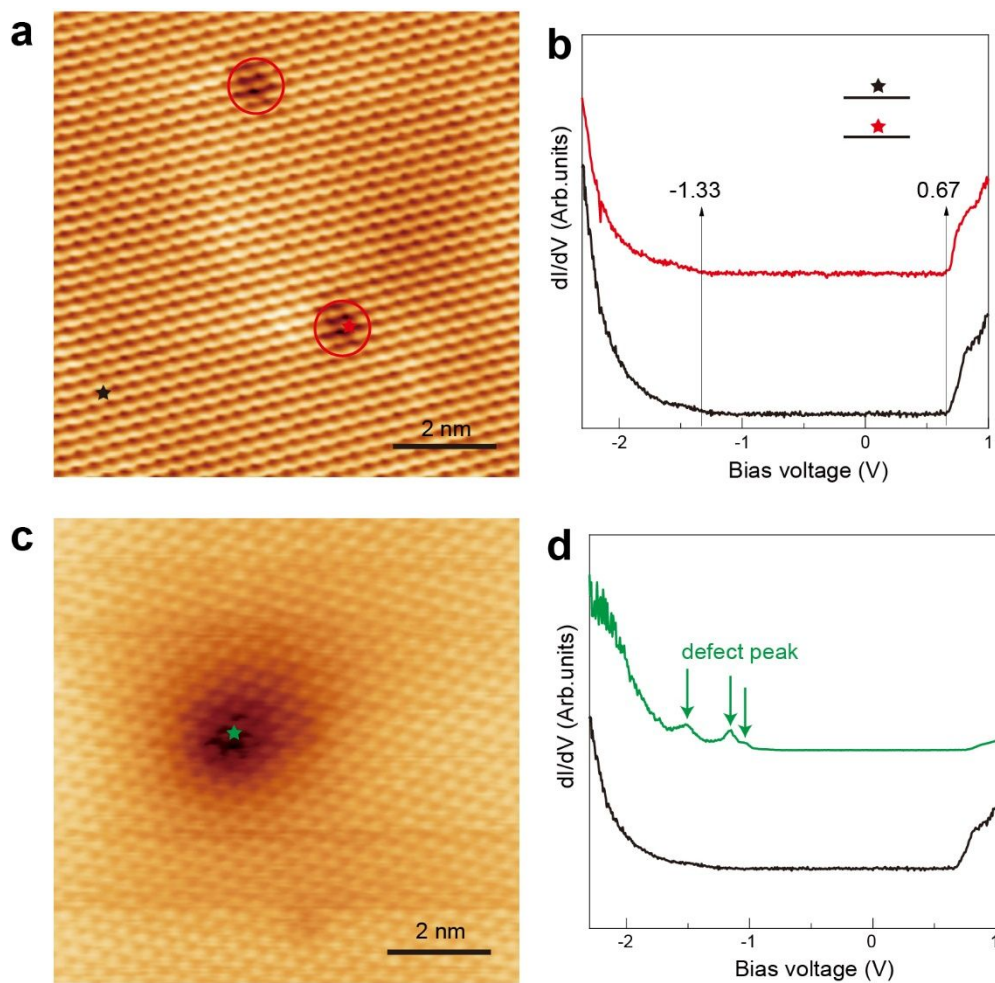


Figure S12. STM image and dI/dV spectrum of two common defects on the surface of 800 K annealing WSe_2 . The defect corresponding to (a) is similar to the oxygen vacancy defect reported in the previous literature^{3,4}, and the defect corresponding to (c) may be a defect formed by the lack of underlying atoms. (a) Sample bias 1 V, tunnel current 2 nA. (c) Sample bias 1.5 V, tunnel current 700 pA.

REFERENCES

- (1) Ugeda, M. M.; Bradley, A. J.; Shi, S.-F.; da Jornada, F. H.; Zhang, Y.; Qiu, D. Y.; Ruan, W.; Mo, S.-K.; Hussain, Z.; Shen, Z.-X.; Wang, F.; Louie, S. G.; Crommie, M. F. Giant Bandgap Renormalization and Excitonic Effects in a Monolayer Transition Metal Dichalcogenide Semiconductor. *Nat. Mater.* **2014**, *13*, 1091-1095.
- (2) Schuler, B.; Qiu, D. Y.; Refaely-Abramson, S.; Kastl, C.; Chen, C. T.; Barja, S.; Koch, R. J.; Ogletree, D. F.; Aloni, S.; Schwartzberg, A. M. Large Spin-Orbit Splitting of Deep in-Gap Defect States of Engineered Sulfur Vacancies in Monolayer WS₂. *Phys. Rev. Lett.* **2019**, *123*, 076801.
- (3) Zheng, Y. J.; Chen, Y.; Huang, Y. L.; Gogoi, P. K.; Li, M.-Y.; Li, L.-J.; Trevisanutto, P. E.; Wang, Q.; Pennycook, S. J.; Wee, A. T. S.; Quek, S. Y. Point Defects and Localized Excitons in 2D WSe₂. *ACS Nano* **2019**, *13*, 6050-6059.
- (4) Barja, S.; Refaely-Abramson, S.; Schuler, B.; Qiu, D. Y.; Pulkin, A.; Wickenburg, S.; Ryu, H.; Ugeda, M. M.; Kastl, C.; Chen, C.; Hwang, C.; Schwartzberg, A.; Aloni, S.; Mo, S.-K.; Frank Ogletree, D.; Crommie, M. F.; Yazyev, O. V.; Louie, S. G.; Neaton, J. B.; Weber-Bargioni, A. Identifying Substitutional Oxygen as a Prolific Point Defect in Monolayer Transition Metal Dichalcogenides. *Nat. Commun.* **2019**, *10*, 3382.